Review

Transition Metal Dichalcogenides Nanoscrolls: Preparation and Applications

Shilong Yu , Pinyi Wang , Huihui Ye , Hailun Tang , Siyuan Wang , Zhikang Wu , Chengjie Pei , Junhui Lu , Hai Li *

Posted Date: 21 July 2023

doi: 10.20944/preprints202307.1431.v1

Keywords: TMDCs; nanosheet; nanoscroll; preparation; photodetection; hydrogen evolution reaction; gas sensing

Review

Transition Metal Dichalcogenides Nanoscrolls: Preparation and Applications

Shilong Yu, Pinyi Wang, Huihui Ye, Hailun Tang, Siyuan Wang, Zhikang Wu, Chengjie Pei, Junhui Lu and Hai Li *

Key Laboratory of Flexible Electronics (KLOFE) & Institute of Advanced Materials (IAM), Nanjing Tech University, Nanjing 211816, China

* Correspondence: iamhli@njtech.edu.cn

Abstract: Two-dimensional (2D) transition metal dichalcogenides (TMDCs) nanosheets have shown extensive applications due to their excellent physical and chemical properties. However, the low light absorption efficiency limits their application in optoelectronics. By rolling up 2D TMDCs nanosheets, the one-dimensional (1D) TMDCs nanoscrolls are formed with spiral tubular structure, tunable interlayer spacing and opening ends. Due to their increased thickness of scroll structure, the light absorption is enhanced. Meanwhile, the rapid electron transportation is confined along the 1D structure. Therefore, the TMDCs nanoscrolls show improved optoelectronic performance compared to 2D nanosheets. In addition, the high specific surface area and active edge site from bending strain of basal plane make them promising materials for catalytic reaction. Thus, the TMDCs nanoscrolls have attracted intensive attention in recent years. In this review, the structure of TMDCs nanoscrolls is firstly demonstrated and followed by various preparation methods of the TMDCs nanoscrolls. Afterwards, the applications of TMDCs nanoscrolls in the fields of photodetection, hydrogen evolution reaction, and gas sensing are discussed.

Keywords: TMDCs; nanosheet; nanoscroll; preparation; photodetection; hydrogen evolution reaction; gas sensing

1. Introduction

As representative two-dimensional (2D) materials, the transition metal dichalcogenides (TMDCs) nanosheets have been successfully applied in the fields of photodetection, energy storage, catalysis, and so on. Although the monolayer TMDCs nanosheets have showed excellent optoelectronic performance, their low light absorption efficiency hinders the applications in photodetection [1], because of their ultrathin thickness.

A great deal of effort has been developed to improve the light absorption of TMDCs nanosheets, such as plasma treatment, formation of van der Waals heterojunction, utilization of plasmonic effect, integration of quantum dots [2–6], etc. Recently, rolling up the monolayer TMDCs nanosheet to form the TMDCs nanoscroll (TMDCs-NS) has been reported as a promising method to improve their optoelectronic performance [3]. With the aid of volatile organic solvents or alkaline solution [3,7–11], the monolayer TMDCs nanosheets can be transformed into one-dimensional (1D) nanoscrolls with tubular and spiral structure [7,12,13]. The as-obtained TMDCs nanoscrolls (TMDCs-NS) showed enhanced light absorption due to the increased cross section. In addition, the TMDCs-NS also inherits the excellent properties from the monolayer TMDCs nanosheet [5,14–19]. Furthermore, the curved structure of nanoscroll exhibits strain, which can modulate the band gap of TMDCs nanosheet [17]. Moreover, its scrolled structure has tunable interlayer space with open ends, in which other functional nanomaterials can be encapsulated [19,20]. Therefore, the TMDCs-NS have attracted great attention in optoelectronics in recent years.

In this review, we introduce the structure, fabrication, and applications of TMDCs-NS. Firstly, the structure of nanoscrolls is demonstrated. Secondly, the preparation methods of nanoscrolls are

Preprints (www.preprints.org) | NOT PEER-REVIEWED | Posted: 21 July 2023 doi:10.20944/preprints202307.1431.v1

discussed in detail. We then present the applications of TMDCs-NS in the photodetection, sensing, and hydrogen evolution reaction.

2. Structure of TMDCs-NS

Different from other 1D nanomaterials, the nanoscrolls have spiral tubular structure with weak van der Waals (vdW) interaction between adjacent layers, which are transformed from 2D nanosheet, exhibiting open ends and side edges without fusion. To date, various 2D nanosheets can be transformed into nanoscrolls, such as graphene, TMDCs, black phosphorus and h-BN [21–26]. The graphene nanoscroll was discovered in the arc discharge experiment of graphite electrode [27], and confirmed by transmission electron microscopy (TEM) [28]. The large scale preparation of graphene nanoscroll was proposed in 2003 and then received much attention [29,30].

Similar to graphene nanoscroll, the TMDCs-NS is also composed of monolayer TMDCs nanosheets scrolled up into Archimedean helical structure (Figure 1b) [21,31]. These TMDCs-NS has unique physical and chemical properties due to their nanoscale dimensions and high surface area-to-volume ratio, which make them useful in a variety of applications, such as energy storage, catalysis, and optoelectronics [3,11,32–36].

The structure of TMDCs-NS is illustrated by taking MoS_2 nanoscroll as an example. By scrolling a monolayer MoS_2 nanosheet (Figure 1a), the MoS_2 nanoscroll is formed with an inner layer radius of R_{in}, an outer layer radius of R_{out}, and a interlayer spacing of h, as shown in Figure 1b [37,38]. The scrolling direction is usually along armchair or zigzag orientation of the MoS_2 nanosheet (Figure 1c) [37]. MD simulation was performed to understand the scrolling direction of MoS_2 at the molecular level (Figure 1d). The results indicate that the energy per atom of nanoscrolls along the armchair orientation is lower than those of nanoscrolls through the zigzag and chiral orientations (Figure 1e). As a consequent, the armchair orientation (Mo-S bond direction) is the dominant trend to roll up the MoS_2 nanosheet into MoS_2 nanoscrolls [39]. The spacing between adjacent layers of MoS_2 nanoscroll also plays important role in determining its stability. As the interlayer spacing increases from 4 to 5.5 Å, the energy of each atom decreases quickly (Figure 1f). While it increases continuously as the interlayer spacing increases from 5.5 to 10 Å. The MoS_2 nanoscroll is in an energy favorable state when the interlayer spacing is in the range of 4.7 ~ 6.5 Å [31,37].

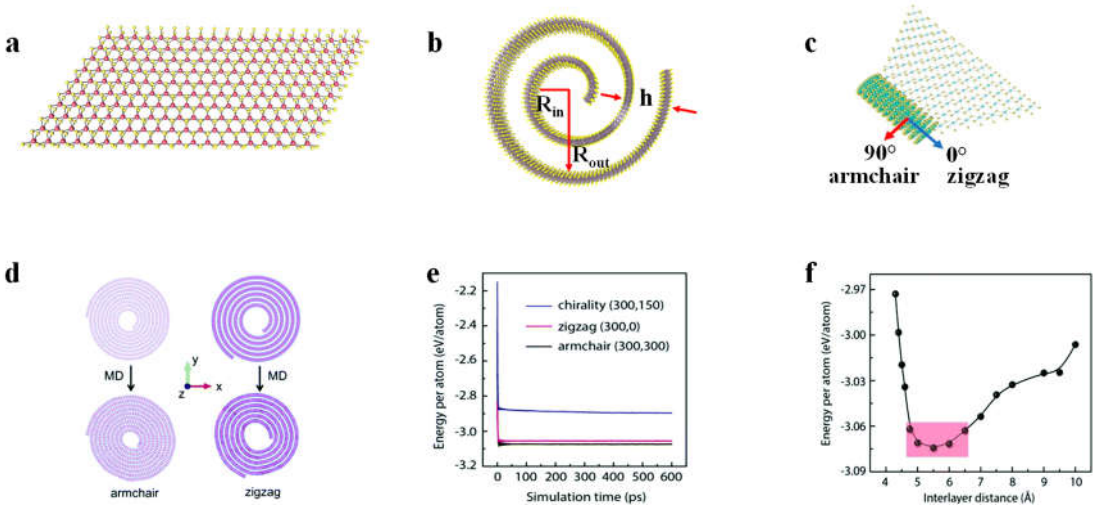

Figure 1. (a) Monolayer MoS_2 nanosheet. (b) The MoS_2 nanoscroll with inter core radius R_{in}, in outer radius R_{out} and interlayer spacing h. (c) The formation of the MoS_2 nanoscrolls are always along the armchair direction (Mo–S bond direction) [39]. (d) The MoS_2 sheets of the same size roll through the armchair (left) and zigzag (right) orientation MD simulations before (upper) and after (lower) structural relaxation [37]. (e) The relationship between unit atomic energy and simulation time of MoS_2 nanoscrolls with armchair, zigzag and chiral orientation [37]. (f) The atomic energy is a function of MoS_2 nanoscrolls spacing. The red area indicates the energy favorable interlayer distance [37].

 doi:10.20944/preprints202307.1431.v1

Preprints (www.preprints.org) | NOT PEER-REVIEWED | Posted: 21 July 2023 doi:10.20944/preprints202307.1431.v1

3. Preparation of TMDCs nanoscrolls

In recent years, many TMDCs nanosheets have been reported to form TMDCs-NS, including MoS_2, WS_2, $MoSe_2$, MoS_2/WS_2, etc [2–4,13,17,35–37,40–54]. A number of methods have been successfully developed to prepare TMDCs-NS, such as strain-induced scrolling [54], argon plasma-assisted scrolling [2], supercritical fluid-assisted scrolling [53,55], volatile organic solvent-induced scrolling [7–9,17,56], alkaline droplet assisted scrolling [3,5,10,11,19], and vortex flow device (VFD) induced continuous flow [34].

Theoretical investigation indicates that there is an energy barrier between the nanosheet and nanoscroll [57–59]. A driving activation energy is required to initialize the scrolling automatically [60]. By scrolling or folding the nanosheet into nanoscroll, the lowest energy form is presented [60]. The barrier can be overcome with the help of external force in liquid or in air, where the TMDCs-NS is formed.

3.1. Fabrication of TMDCs nanoscrolls in liquid

3.1.1. Solvent evaporation to make nanoscrolls

Many organic solvents are liquid at ambient conditions with large volatility, which can be used to assist or induce the scrolling of TMDCs nanosheets [7,17,19,61–63], such as acetone, ethanol, and isopropanol [8,64–66]. In 2018, we proposed the preparation of MoS_2 nanoscroll by dropping an ethanol or acetone droplet on monolayer MoS_2 nanosheet [7], as shown in Figure 2. Monolayer MoS_2 nanosheets were firstly obtained by chemical vapor deposition (CVD) on SiO_2/Si (Figure 2a and 2b), and a drop of ethanol was deposited on the MoS_2 nanosheets (Figure 2c). Due to its low surface tension, the ethanol can wet MoS_2 and SiO_2/Si substrates easily. During the evaporation process, a thin ethanol layer is formed near the contact line (Figure 2d). With the rapid evaporation of ethanol, a temperature gradient is generated near the contact line, creating a surface tension gradient to induce fluid flow. Such kind of fluid flow could roll up the edge of MoS_2. As the contact line moves, the MoS_2 nanosheet continue to be rolled up until a complete MoS_2 nanoscroll is formed (Figure 2e) [7].

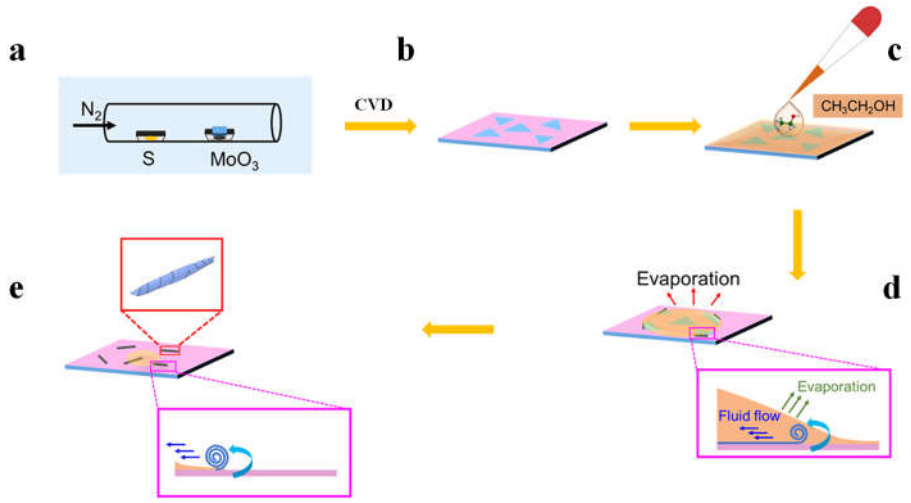

Figure 2. Volatile organic solvent-assisted fabrication of MoS_2 nanoscroll [7]. (a-b) CVD growth of monolayer MoS_2 nanosheets. (c) A drop of ethanol is deposited on MoS_2 nanosheets. (d) The edges of MoS_2 nanosheets are rolled up during the evaporation of ethanol. (e) MoS_2 nanoscrolls were formed.

By dropping the mixture of ethanol and water on CVD-grown monolayer MoS_2 nanosheet, Jian Zheng et al. also successfully prepared MoS_2 nanoscrolls, as shown in Figure 3 [8]. Large-area monolayer MoS_2 nanosheets were obtained firstly by CVD (Figure 3a). MoS_2 nanoscrolls were then fabricated in short time in a mixture solution of ethanol and water with a volume ratio of 2:1 (ethanol: water = 2:1).

Preprints (www.preprints.org) | NOT PEER-REVIEWED | Posted: 21 July 2023 doi:10.20944/preprints202307.1431.v1

Due to the high temperature caused mismatch between the MoS_2 nanosheet and substrate during CVD growth (Figure 3a), a strain equilibrium is balanced between them when the temperature decreased to room temperature (Figure 3b). When the mixture solution is dropped onto the MoS_2 nanosheet, the ethanol intercalates between the MoS_2 and substrate, and the upper part of MoS_2 is detached from the substrate. In this case, the strain balance is broken (Figure 3c), and the released portion curls into a roll (Figure 3d). Due to the adhesion from substrate, the left portion remains intact [5]. With the evaporation of ethanol, the surface tension at the air-solvent-MoS_2 interface is greater than that between MoS_2 and substrate. As a result, the strain-adhesion balance is broken continuously, generating MoS_2 nanoscroll finally (Figure 3e).

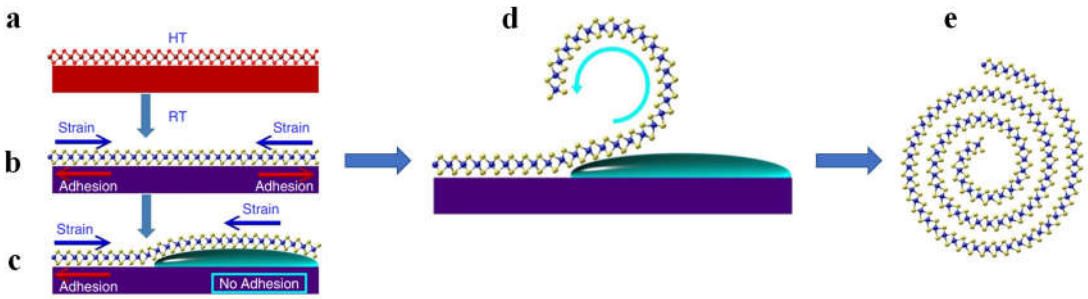

Figure 3. The mixture of ethanol and water assisted fabrication of MoS_2 nanoscroll [8]. (a) CVD growth of MoS_2 nanosheet. (b) Strain-balanced MoS_2 on substrate. (c) After ethanol intercalation, the strain-adhesion balance between MoS_2 and substrate is broken. (d) Rolling up the edge of MoS_2 nanosheet. (e) The as-prepared MoS_2 nanoscroll.

3.1.2. Alkaline droplet-assisted fabrication of nanoscrolls

For bilayer and multilayer nanosheets, it is difficult to roll them up effectively due to the strong adhesion force from the substrate. Since TMDCs nanosheets are usually grown on SiO_2/Si substrate, etching the SiO_2 layer beneath them could eliminate the strong adhesion from the substrate. Therefore, alkaline solution has been used to etch the SiO_2 layer, and thus break the adhesion energy between the nanosheet and substrate (Figure 4). As a result, the strain equilibrium is broken, rolling up the TMDCs nanosheet from edges to form spiral nanoscrolls [3,35].

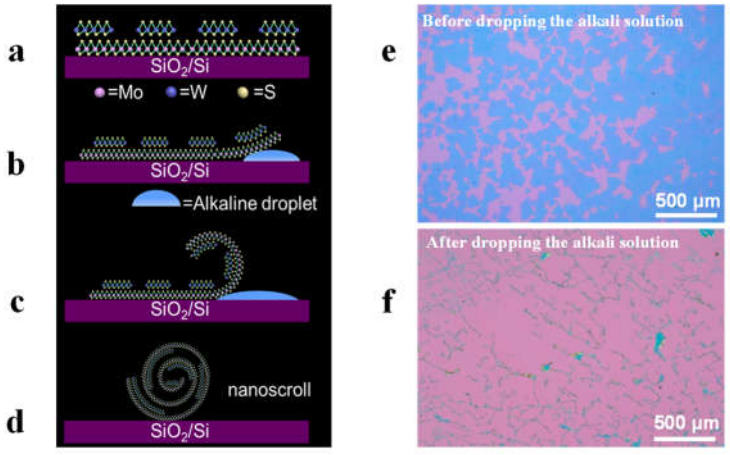

Figure 4. Alkaline droplet-assisted fabrication of nanoscrolls [3]. (a) CVD-grown MoS_2/WS_2 heterostructures nanosheet on SiO_2/Si substrate. (b) Etching the SiO_2 layer beneath the nanosheet by dropping alkaline solution. (c) The edge of WS_2/MoS_2 nanosheet is rolled up due to the elimination of strong adhesion from substrate. (d) The as-formed WS_2/MoS_2 heterojunction nanoscroll. (e-f) Show the comparison before and after dropping the alkali solution on the MoS_2/WS_2 nanosheets.

Preprints (www.preprints.org) | NOT PEER-REVIEWED | Posted: 21 July 2023 doi:10.20944/preprints202307.1431.v1

In 2020, we proposed a method to scroll MoS_2/WS_2 heterostructures nanosheet by using alkaline solution. Firstly, large area MoS_2/WS_2 heterostructures nanosheet were grown on SiO_2/Si substrate by CVD (Figure 4a). Afterwards, 50μL of alkaline aqueous solution (0.1 M KOH or $NaHCO_3$) was dropped on the nanosheets. The SiO_2 layer was etched by the alkaline solution, allowing penetration of alkaline solution into the interface of nanosheet and SiO_2/Si substrate (Figure 4b), which could further etch the SiO_2 layer to release the edge of nanosheet. To decrease the energy form, the released edge of nanosheet tends to be scrolled (Figure 4c). With the further etching of SiO_2 layer, more portion of nanosheet was released and continuously scrolled till forming nanoscroll (Figure 4c and 4d) [3]. The as-obtained nanoscroll was then rinsed with deionized (DI) water and dried with N_2 for characterization and device fabrication (Figure 4d). Besides MoS_2/WS_2 heterostructures nanosheet, we found that the silver nanoparticles decorated monolayer MoS_2 and WS_2 nanosheets could also be rolled up effectively by using alkaline solution [19].

Duan et al. found that 80% of the bilayer and trilayer TMDCs heterostructure nanosheets could be transformed into 1D nanoscrolls by using mixture of ethanol and water. However, many scrolls are incompletely rolled up with tightly pinned edges, indicating the mixed solvent doesn't work well to completely delaminate the edges of thick 2D nanosheet. While the yield of nanoscroll increased to 90% by adding 5% ammonia into the mixed solvent, with 60% of them showing closely-stacked scroll structure. The result indicated that the etching of SiO_2 layer by alkaline solution played important role in peeling off 2D nanosheet from substrate even the existence of strong edge-substrate interaction [5,8].

Similarly, alkaline solution was also employed to roll up PbI_2/MoS_2 and $BaTiO_3/MoS_2$ nanosheets into complete nanoscroll, further confirming the importance of alkaline solution in preparation of TMDCs-NS [11,35,48].

3.1.3. Fabrication of TMDCs nanoscrolls by dragging water droplets

Due to the low surface tension of organic solvent, it is easily adsorbed on TMDCs nanosheets. Thus, it is inevitable to trap organic solvent into the TMDCs-NS during the scrolling process. It is known that the adsorbed organic solvent could greatly influence the properties and device performance of TMDCs nanosheets. Therefore, it is desirable to fabricate TMDCs-NS without using organic solvent. Recently, we reported an organic solvent-free method to fabricate tightly-packed TMDCs-NS [36]. Firstly, CVD-grown monolayer MoS_2 nanosheets were heated at 100 °C, as shown in Figure 5a and 5b. After 3μL deionized (DI) water droplet was dropped on the MoS_2 nanosheets (Figure 5c), it was dragged from one end to the other at a speed of 3mm/s (Figure 5d). Afterwards, large scale closely packed MoS_2 nanoscrolls were fabricated (Figure 5e).

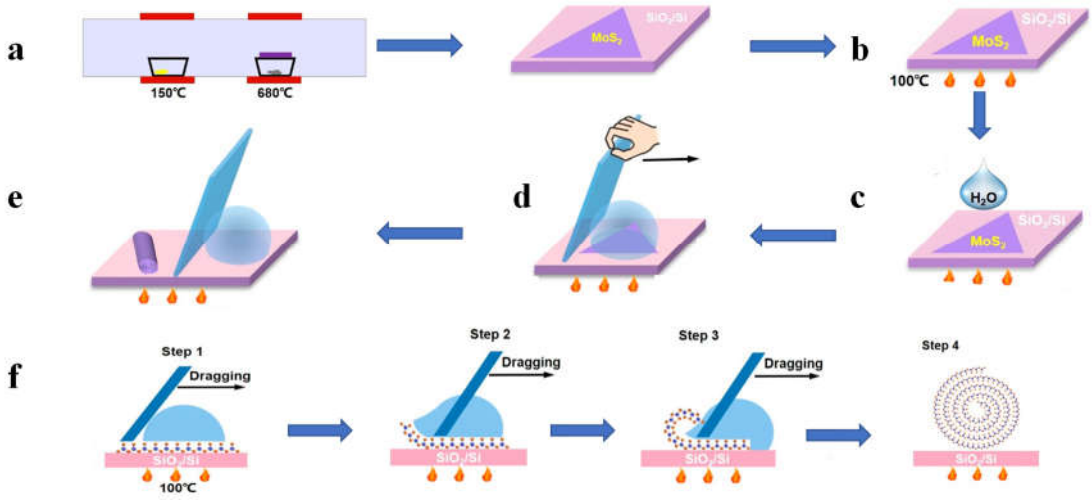

Figure 5. Fabrication of TMDCs nanoscrolls by dragging water droplet at 100 °C [36]. (a) Monolayer MoS_2 nanosheet was grown by CVD at 680 °C. b. Heat the substrate and MoS_2 nanosheets for 10 min. c. A drop of H_2O on the MoS_2 film. d. The H_2O droplet was dragged across the MoS_2 nanosheet

Preprints (www.preprints.org) | NOT PEER-REVIEWED | Posted: 21 July 2023 doi:10.20944/preprints202307.1431.v1

on the SiO_2/Si substrate by a coverslip at 3 mm/s^{-1}; e. MoS_2 nanoscroll was formed after removing the H_2O droplet; f. Schematic diagram of the formation of the MoS_2-NS.

The detailed mechanism for the formation of nanoscrolls could be explained as follows, as shown in Figure 5f. When the monolayer MoS_2 nanosheets on SiO_2/Si substrate was heated at 100°C, the adhesion force between the nanosheets and substrate was weakened. Therefore, with the movement of water droplet, the scrolling occurs first at the edges of MoS_2 nanosheets. Due to the hydrophobicity of MoS_2 nanosheets, the low friction between water and MoS_2 and the high surface tension of water contribute to the following scrolling of MoS_2 nanosheets. More importantly, due to the hydrophobicity of MoS_2, the water molecules were difficult to be trapped into the nanoscolls, obtaining solvent-free and closely-packed nanoscrolls [36].

3.1.4. Amine-functional amphiphilic molecule assisted fabrication of TMDCs nanoscrolls

The involvement of amphiphilic molecules in the preparation of MoS_2, $MoSe_2$, and $MoTe_2$ nanoscrolls has also been investigated [32,33,67,68]. By mixing N-(2-aminoethyl)-3α-hydroxy-5β-cholan-24-amide (LCA) and exfoliated TMDCs nanosheets in orthodichlorobenzene (ODCB) for 24 hours at room temperature, TMDCs-NS was obtained in large scale (Figure 6a). The formation of MoS_2 nanoscrolls with the help of LCA could be explained as follows. Firstly, the LCA molecules were self-assembled into fibers in ODCB. The amine group of LCA fiber has stronger interaction with edges of TMDCs nanosheets than the entire plane. Thus, the edges starts scrolling around the LCA fibers. With the gradual self-assembly of LCA fiber, the interaction of fiber with edges of TMDCs nanosheets is enhanced. In this case, the original equilibrium state of TMDCs nanosheets is broken and the nanosheet scrolls spontaneously. Therefore, TMDCs-NS was formed. By using this method, MoS_2 nanoscrolls, MoS_2-Ag nanoparticles nanoscrolls, and MoS_2-Au nanoparticles nanoscrolls have successfully prepared [33,68].

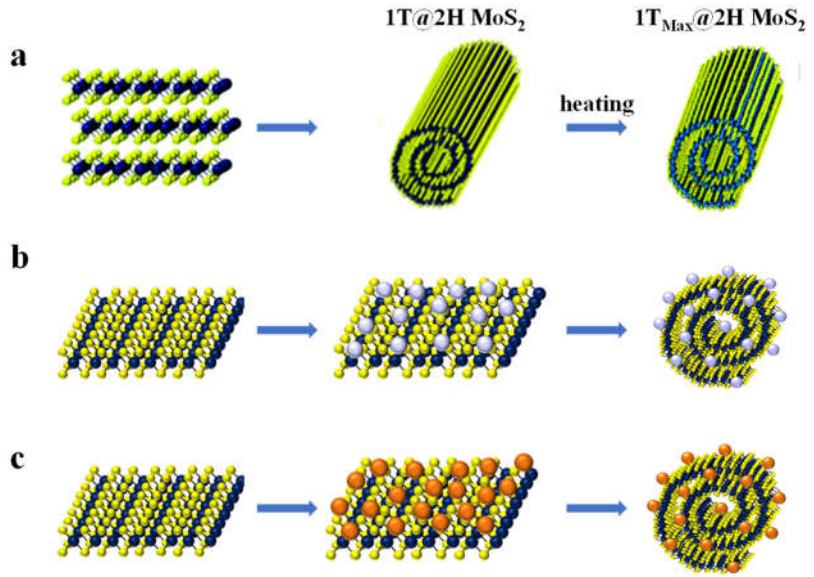

Figure 6. Amine-functional amphiphilic molecule assisted fabrication of TMDCs nanoscrolls. (a) Scheme of Amine-functional amphiphilic molecule assisted fabrication of 1T@2H MoS_2 nanoscrolls [33]. (b-c) Scheme of Amine-functional amphiphilic molecule assisted fabrication of MoS_2-Ag and MoS_2-Au nanoscrolls [68].

3.1.5. Supercritical fluid assisted fabrication of nanoscrolls

Supercritical fluids (SCFs) are fluids with much more space and highly compressible than ordinary fluids above their critical temperatures and pressure [69,70]. By controlling the temperature or pressure, the density and solvent strength of SCFs can be tuned from gas-like to solid-like [33,68,71,72]. SCF has unique properties such as gas diffusivity, liquid solubility, low interfacial

Preprints (www.preprints.org) | NOT PEER-REVIEWED | Posted: 21 July 2023 doi:10.20944/preprints202307.1431.v1

tension, excellent surface wettability, and high diffusion coefficient [73–75]. Thus, the SCFs processing have been used as a promising and effective route to exfoliate layered materials into 2D nanosheets, such as graphene, BN, and MoS_2 due to their simplicity, rapidity, and short reaction time [53,55,73,76]. It has been reported that the as-exfoliated 2D nanosheets can be rolled up into nanoscrolls in order to minimize their surface energy. Therefore, MoS_2 and WS_2 nanoscrolls can be formed by using SCF processing of MoS_2 nanosheets in 30 minutes, as shown in Figure 7 [53,73]. The X-ray diffraction (XRD) patterns of the MoS_2 nanoscrolls clearly show that the surfaces of the MoS_2 nanosheets are not oxidized and are free of impurities [53]. Meanwhile, the lattice structure of the SCF-prepared MoS_2 is essentially unchanged, making this method a convenient and efficient way to prepare nanoscrolls.

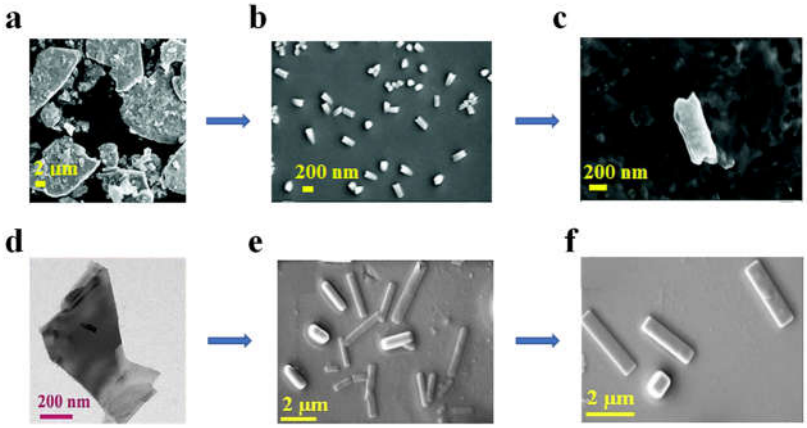

Figure 7. Supercritical fluid processing-assisted fabrication of TMDCs nanoscrolls. FE-SEM images of (a) bulk MoS_2 flake and (b–c) supercritical fluid prepared MoS_2 nanoscrolls [73]. FE-SEM images of (d) bulk WS_2 flake and (e–f) supercritical fluid prepared WS_2 nanoscrolls [53].

3.1.6. Shear force assisted fabrication of nanoscrolls

By using vortex flow device (VFD), MoS_2 nanosheets have been successfully transformed into nanoscrolls under continuous flow [34]. In a tilted quartz tube with rapid rotation, dynamic thin film was generated in VFD, providing mechanoenergy as high shear stress during intense micro-mixing. Therefore, the MoS_2 nanosheets were firstly exfoliated from bulk material due to the strong shear stress. Simultaneously, the as-exfoliated MoS_2 nanosheets were rolled up in-situ to form scrolls with high yield (Figure 8a-b). At low-speed rotation (4000 rpm), the shear stress is mainly governed by the Typhoon-like toroidal flow, generating centrifugal forces on the tube wall. As a result, the MoS_2 nanosheets were exfoliated firstly and then scrolled as the toroidal flow moves upwards (Figure 8c-d) [34,77,78]. As the rotation speed increased to 8000 rpm, the dominated double-helical twisted Faraday wave vortex flow cannot curl and roll up MoS_2 nanosheets effectively. The morphology of MoS_2 nanostructure can be changed from lamellae to scroll, by controlling the solvent selection, concentration of bulk material, and the processing parameters of VFD, including rotation speed and rotation angle. The VFD has been widely used to synthesize nanoscrolls from 2D nanosheets, such as graphite, graphene oxide, and hexagonal boron nitride [77–79].

Preprints (www.preprints.org) | NOT PEER-REVIEWED | Posted: 21 July 2023 doi:10.20944/preprints202307.1431.v1

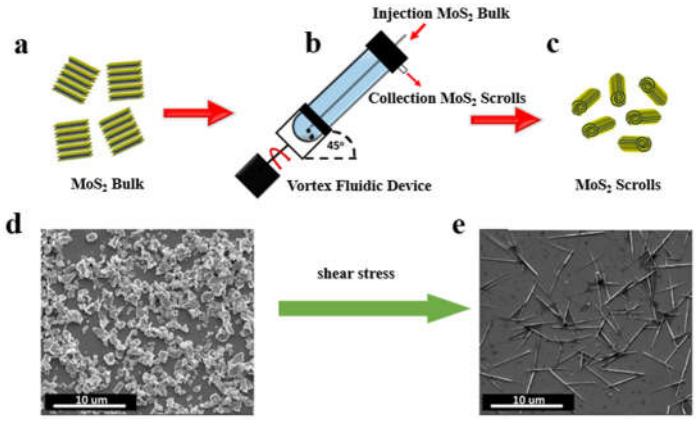

Figure 8. Shear force assisted fabrication of nanoscrolls [34]. (a-c) Schematic illustration of the fabrication of MoS_2 scrolls in VFD. SEM images of the (d) MoS_2 bulk material and (e) as-prepared MoS_2 scrolls in VFD.

3.2. Fabrication of TMDCs nanoscrolls in air

3.2.1. Plasma-assisted fabrication of MoS_2 nanoscrolls

In 2016, Zhang et al. proposed preparation of MoS_2 nanoscrolls by treating CVD-grown monolayer MoS_2 nanosheets in a weak Ar plasma environment, as shown in Figure 9 [2]. Upon plasma bombardment, the top layer sulfur atoms of the MoS_2 nanosheets are partially removed as the kinetic energy of Ar^+ is larger than the binding energy of Mo-S bond. As a result, the MoS_2 lattice is disrupted and unsaturated dangling bonds are left, leading to out-of-plane strain. Such kind of strain induces out-of-plane distortion, which rolls up the edge of MoS_2 nanosheet to form nanoscrolls [2,41]. The optimum power for fabricating nanoscrolls was 25 W. If the power was too strong, short nanoscrolls were obtained. While longer time was needed to trigger the scrolling when the power was too weak. When the adjacent edges of MoS_2 nanosheets are not parallel, a kink will be formed, preventing the formation of long scroll [2]. In addition, WS_2 and WSe_2 nanoscrolls were also prepared by treating the monolayer WS_2 and WSe_2 nanosheets in Ar plasma.

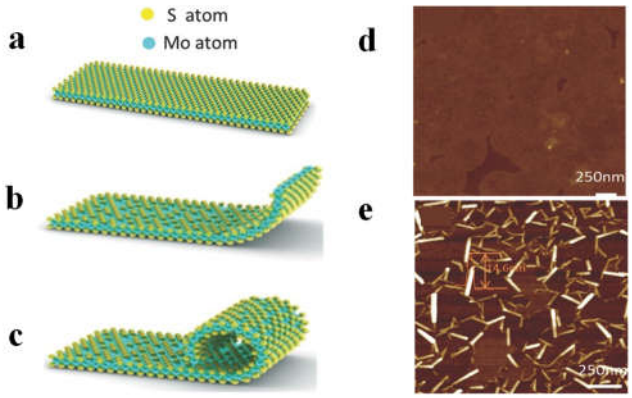

Figure 9. Ar plasma-assisted fabrication of MoS_2 nanoscrolls [2]. Schematic structures of (a) monolayer, (b) edge distortion, and (c) scrolled edge of MoS_2 nanosheet under Ar plasma treatment. AFM images of (d) monolayer MoS_2 nanosheet and (e) as-obtained MoS_2 nanoscrolls.

3.2.2. Strain-assisted fabrication of TMDCs nanoscrolls

Because of the different thermal expansion coefficients of the MoS_2 and SiO_2, there are thermal strain gradients between the interface of CVD-grown MoS_2 nanosheets and SiO_2/Si substrate [41,61,80]. Upon quenching, the orientation-specific fractures are formed on CVD-grown MoS_2 nanosheets due to the existed S vacancies (Figure 10a-b). Since the cooling rate of top MoS_2 layer is

Preprints (www.preprints.org) | NOT PEER-REVIEWED | Posted: 21 July 2023 doi:10.20944/preprints202307.1431.v1

greater than the bottom SiO_2 layer, strong lattice contraction of MoS_2 layer is observed due to the temperature difference, which induces self-curling at the fractures of MoS_2 layer (Figure 10c). Afterwards, the curled edge continues to form scroll in order to minimize the surface energy (Figure 10d).

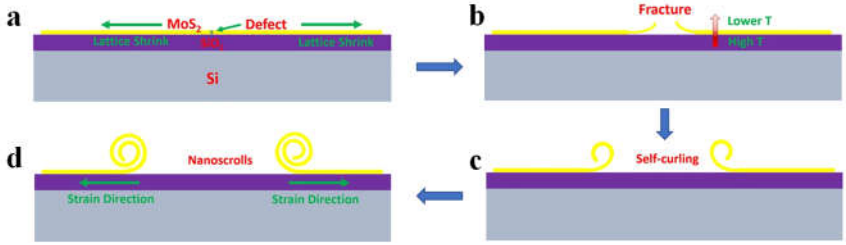

Figure 10. Schematic diagram of nanoscroll formed by thermal strain [81]. (a) Monolayer MoS_2 nanosheets were prepared on SiO_2/Si substrate by CVD. (b) S vacancy acts as crack nuclei due to the thermal strain upon quenching. (c) Self-curling at the fractures of MoS_2 layer because of the temperature difference between MoS_2 and SiO_2 layer. (d) The MoS_2 nanoscroll formed by thermal strain.

Table 1 summarizes the preparation methods of TMDCs nanoscrolls to show the advantages and disadvantages in detail.

Table 1. The advantages and disadvantages of preparation methods for TMDCs nanoscrolls.

	Methods	Advantages	Challenges	References
In liquid	Solvent evaporation to make nanoscroll	Large area, large size, high productivity, short time consuming, easy to operate	Solvent residue, loose nanoscrolls	[6–9,17,37,39,52,56,65,82]
	Alkaline droplet-assisted fabrication of nanoscroll	High yield, high productivity for thick nanosheet	Substrate etching, solvent residue	[3,5,10,11,19,35]
	Fabrication of TMDCs nanoscroll by dragging water droplet	High yield, solvent-free residue, tightly packed nanoscroll	Not suitable for water and oxygen sensitive material	[36]
	Amine-functional amphiphilic molecule assisted fabrication of TMDCs nanoscroll	High yield, easy to operate	Small dimension, solvent residue	[32,33,67]
	Supercritical fluid assisted fabrication of nanoscroll	Simple, fast	Small dimension, solvent residue	[73]
	Shear force assisted fabrication of nanoscroll	High productivity, easy to operate	Low proportion of monolayer nanosheet	[34]
In air	Plasma-assisted fabrication of TMDCs nanoscroll	Simple process, high yield	Small dimension, structure damage	[2,4]
	Strain-assisted fabrication of TMDCs nanoscroll	Simple and repeatable	Complex process, low productivity, incomplete nanoscroll	[54]

4. Applications of TMDCs-NS

4.1. Photodetector based on TMDCs-NS

Compared to monolayer TMDCs nanosheet, the TMDCs-NS shows much better light absorption efficiency due to its increased thickness of spirally scrolled structure. Thus, the TMDCs-NS should exhibit excellent optoelectronic performance. Recently, the photodetection performance of TMDCs-NS has been investigated [35,83]. Photosensitivity, described by the ratio of photocurrent to dark

Preprints (www.preprints.org) | NOT PEER-REVIEWED | Posted: 21 July 2023 doi:10.20944/preprints202307.1431.v1

current (PDR), is one of the most important parameters to evaluate the performance of a photodetector [3,7,19]. Figure 11a shows the PDRs of MoS_2 nanosheet and nanoscroll based photodetectors under blue light irradiation with a bias voltage of 0.1 V. The PDR of nanoscroll based photodetector is about 400, which is about 100 times higher than that of nanosheet based one [7]. In addition, the response and recovery time of nanoscroll based photodetector are less than the nanosheet based photodetector. Similar enhanced PDR was also observed in the $MoSe_2$ nanoscroll based device [54]. These results indicate that the TMDCs-NS shows much better photodetection performance than the TMDCs nanosheet, which should be attributed to the enhanced light absorption and rapid electron transportation along 1D structure [8,36]. Moreover, due to the large surface to volume ratio of MoS_2 nanosheet, the adsorbates, such as O_2 and H_2O molecules, greatly reduce the photoresponse of MoS_2 nanosheet based device. While the MoS_2 nanoscroll has much smaller surface to volume ratio than nanosheet, which can decrease the influence of adsorbates on the photoresponse.

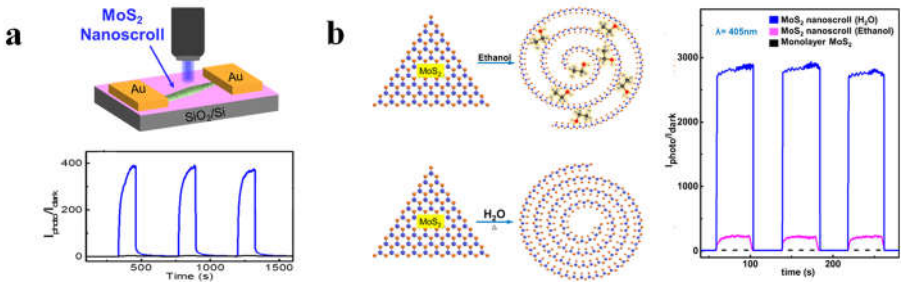

Figure 11. Photodetection performance of TMDCs-NS based device. (a) Top panel: Scheme of photodetector based on MoS_2 nanoscroll. Bottom panel: PDR plot of photodetectors based on MoS_2 nanosheet and nanoscroll under 405 nm laser [7]. (b) The scheme of nanoscrolls made by dropping ethanol and water droplets, respectively. PDR plot of corresponding photodetectors under 405 nm laser [36].

Compared to the MoS_2 nanoscroll prepared by ethanol droplet (MoS_2 NS-ethanol), the MoS_2 nanoscroll prepared by water droplet (MoS_2 NS-water) shows higher PDR (Figure 11 b) [36]. The ethanol molecules trapped in MoS_2 NS-ethanol reduce the light absorption and hinder the interlayer transport of photogenerated carriers, and thus decrease the photoresponse. In addition, the ethanol can donate electron to MoS_2 and thus increase the dark current of MoS_2 NS-ethanol, which in turn decrease the PDR. Moreover, the MoS_2 NS-water shows a slightly higher photocurrent than MoS_2 NS-ethanol.

4.2. Photodetector based on TMDCs-NS composite

In bilayer WS_2/MoS_2 heterostructure, the carriers can be transferred from MoS_2 to WS_2 within 50 fs under illumination, indicating the important role of interface. However, there is only one interface in bilayer WS_2/MoS_2 heterostructure. The photoresponse performance of WS_2/MoS_2 heterostructure could be further improved if multiple interfaces can be established. By scrolling bilayer WS_2/MoS_2 heterostructure into WS_2/MoS_2 heterostructure nanoscroll, multiple hetero-interfaces are formed, which could show better photoresponse than the bilayer WS_2/MoS_2 heterostructure with one hetero-interface. After bilayer WS_2/MoS_2 heterostructure was grown by CVD, the alkaline droplet was dropped on it to roll up the bilayer heterostructure into nanoscroll [3]. As shown in Figure 12a, the PDR of bilayer WS_2/MoS_2 heterostructure based photodetector is ~180 under blue laser, which is much higher than that of monolayer MoS_2 or WS_2 nanosheets. While the PDR of WS_2/MoS_2 heterostructure nanoscroll based photodetector is 2700, about an order of magnitude higher than that of bilayer WS_2/MoS_2 heterostructure based photodetector.

By encapsulating photoactive PbI_2 nanocrystals into MoS_2 nanoscroll, the PDR of MoS_2 nanoscroll can be enhanced by two orders of magnitude (Figure 12 b) [48]. Similarly, the PDRs of MoS_2 and WS_2 nanoscroll also increased by two orders of magnitude after Ag nanoparticles were

Preprints (www.preprints.org) | NOT PEER-REVIEWED | Posted: 21 July 2023 doi:10.20944/preprints202307.1431.v1

trapped into nanoscroll (Figure 12c) [19]. Moreover, the photoresponsivity of MoS_2 nanoscroll was also enhanced by about two orders of magnitude when $BaTiO_3$ nanoparticles were encapsulated into it [11]. By doping WS_2 nanoscroll with CdSe–ZnS quantum dots, the photosensitivity can be enhanced by 3000-fold (Figure 12d) [65]. Compared to single TMDCs nanoscrolls, the nanoscroll composite shows excellent photodetection performance [8,56], indicating it could be promising candidate for high-performance optoelectronics.

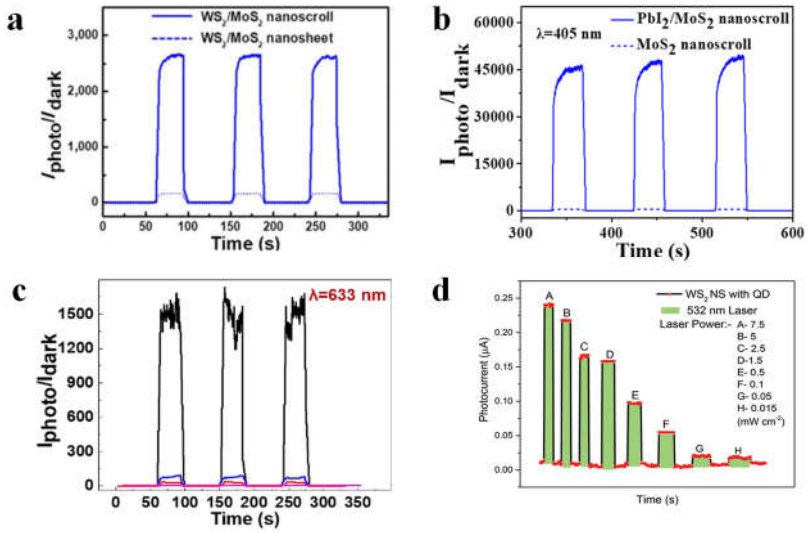

Figure 12. Photodetector based on TMDCs-NS composite. (a) Plots of the PDRs of photodetectors based on WS_2/MoS_2 nanosheet and nanoscroll under blue laser [3]. (b) PDRs plots of photodetectors based on MoS_2 nanoscrolls and PbI_2/MoS_2 nanoscrolls under 405 nm lasers [48]. c. Plots of the PDRs of the MoS_2 nanosheet, MoS_2 nanoscroll, MoS_2-Ag nanosheet, and MoS_2-Ag NS under a 633 nm laser [19]. d. Photocurrent variations in hybridized WS_2 nanoscroll photodetectors under different power densities of a 532 nm laser [65].

4.3. Hydrogen Evolution Reaction

The conductivity and effective active site of catalyst are two key factors to improve the hydrogen precipitation reaction (HER) [84–86]. TMDCs are considered as promising candidates after noble metals for catalytic hydrogen precipitation due to their good electrical conductivity and abundant active edges [51,87,88]. The introduction of small amount of MoSx greatly enhanced the HER activity of NbS_2 nanoflakes [85]. The theoretical calculation indicates that Mo edge sites are identified as the catalytically active site for HER [89,90].

A number of efforts have been employed to increase the active sites and conductivity of TMDCs materials [91–93]. Among them, transforming the TMDCs nanosheets into nanoscrolls with active edges is of great interest in electrocatalytic HER [34]. By curling the TMDCs nanosheets to form nanoscrolls, the curled edges provide highly active edge sites for efficient catalysis. Meanwhile, the bending strain of basal plane also provides more active sites due to the scrolled structure [34,94–96]. In addition, the specific surface area of nanoscroll increases, converting the solution contact from single-sided contact of the nanosheet to multi-layer contact [97]. As a result, the TMDCs-NS provides higher catalytic activity and better conductivity. Thus, the HER activity of TMDCs-NS is greatly enhanced. Figure 13a shows the polarization curves of metallic WSe_2 (M-WSe_2) and 2H-WSe_2 nanoscrolls compared to the commercial Pt/C catalyst. The M-WSe_2 nanoscroll exhibits higher HER activity, smaller overpotential and larger current densities than the 2H-WSe_2 nanoscroll, attributing to its good conductivity and enhanced catalytic activity from scrolled structure [88]. Figure 13b shows the linear scanning voltammogram curves of current density and potential for Pt electrode, MoS_2 sheet, MoS_2 nanoscroll, MoS_2 nanoscrolls@Pt, MoS_2@Pt sheet, and MoS_2@Pt nanoscroll [32]. The MoS_2 nanosheet shows overpotential over 400 mV, while that of MoS_2 nanoscroll decreases. The

Preprints (www.preprints.org) | NOT PEER-REVIEWED | Posted: 21 July 2023 doi:10.20944/preprints202307.1431.v1

overpotential of MoS_2 nanoscroll decorated by Pt nanoparticles (NPs) greatly decreases, indicating the important role of Pt NPs in enhancing the HER activity. By decorating Pt NPs on MoS_2 nanosheet (MoS_2@Pt sheet), the overpotential further decreases to around 300 mV. After the MoS_2@Pt sheet was rolled up to form MoS_2@Pt scroll, the overpotential is reduced to 200 mV, implying the basal plane bending of nanoscroll can further improve the HER activity.

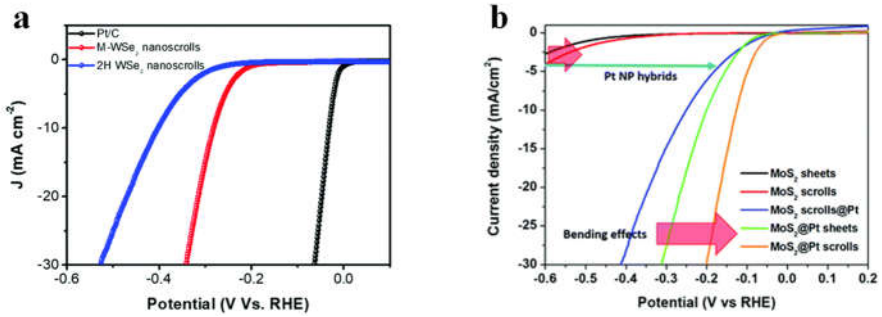

Figure 13. Hydrogen evolution reaction (HER) based on TMDCs-NS. (a) HER polarization curves for M-WSe_2 nanoscrolls, 2H-WSe_2 nanoscrolls, and the commercial Pt/C [88]. (b) Polarization curves for Pt electrode, MoS_2 sheet, MoS_2 nanoscroll, MoS_2 nanoscrolls@Pt, MoS_2@Pt sheet, and MoS_2@Pt nanoscroll [32].

4.4. Gas sensor

In recent years, TMDCs nanosheets have been attracted great attention for gas sensing because of their large surface to volume ratio and good electrical properties [98–101]. The TMDCs nanosheets based gas sensors show high sensitivity for trace gas molecules and good selectivity at room temperature [44,102–104]. However, they suffer from incomplete recovery and poor stability [105], which limit their practical applications. The TMDCs-NS has good conductivity due to its 1D structure and specific surface area from tubular structure. Meanwhile, the nanoscroll structure also provide tunable space to encapsulate functional nanomaterials for further enhanced performance. Therefore, the TMDCs-NS has been considered to present promising performance in the field of gas sensing [106].

By electrochemically exfoliating InSe crystal in electrolyte containing cetyltrimethylammonium bromide (CTAB), the CTAB-functionalized InSe nanosheets (C-InSe) were obtained [105]. With the aid of solvent evaporation, the C-InSe nanosheets rolled up to form C-InSe nanoscroll. After the as-obtained C-InSe nanoscrolls were deposited on interdigitated electrodes (Figure 14b), they were placed into a chamber with fixed concentration of NO_2 gas. An LED lamp illuminates light into the chamber through a glass cover (Figure 14a). The response of C-InSe nanoscrolls based sensor increases under light illumination (Figure 14c). The enhanced response is arisen from the increased adsorption of NO_2 molecules favored by photogenerated electrons. While desorption of NO_2 is observed as the light intensity increases further, which decreases the response of sensor. As the concentration of NO_2 increases from 100 ppb to 25 ppm, the response of C-InSe nanosheets and nanoscrolls based sensors largely increases (Figure 14d). However, the C-InSe nanoscrolls based sensor exhibits much better response than C-InSe nanosheets based sensor, indicating the superiority of nanoscroll in gas sensing.

Preprints (www.preprints.org) | NOT PEER-REVIEWED | Posted: 21 July 2023 doi:10.20944/preprints202307.1431.v1

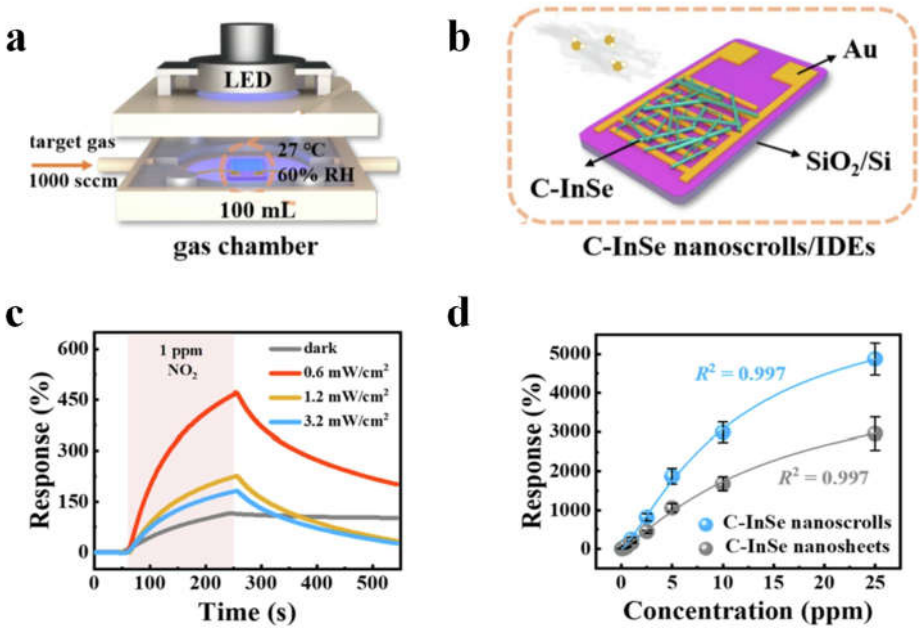

Figure 14. Gas sensor based on C-InSe nanoscrolls [105]. (a-b) Schematic illustration of C-InSe nanoscroll based gas sensor and test platform. (c) Response curves of C-InSe nanoscrolls sensor towards 1 ppm NO_2 under blue light irradiation with different light intensities. (d) Relationship between the response of C-InSe nanosheets and nanoscrolls based sensors and NO_2 concentration.

5. Conclusion

In this review, we summarize a series of fabrication methods of TMDCs nanoscrolls, and briefly demonstrate their applications in photodetection, HER and gas sensing (Figure 15). Compared to 2D TMDCs nanosheet, the 1D TMDCs nanoscroll presents higher light absorption efficiency and faster electron transport because of the scrolled structure. Due to their higher specific surface area and active edges, the TMDCs nanoscrolls have shown excellent performance in catalytic reaction. In conclusion, the TMDCs nanoscrolls are emerging materials with many novel physical and chemical properties that are promising for optoelectronics, catalysis, energy storage, and sensing.

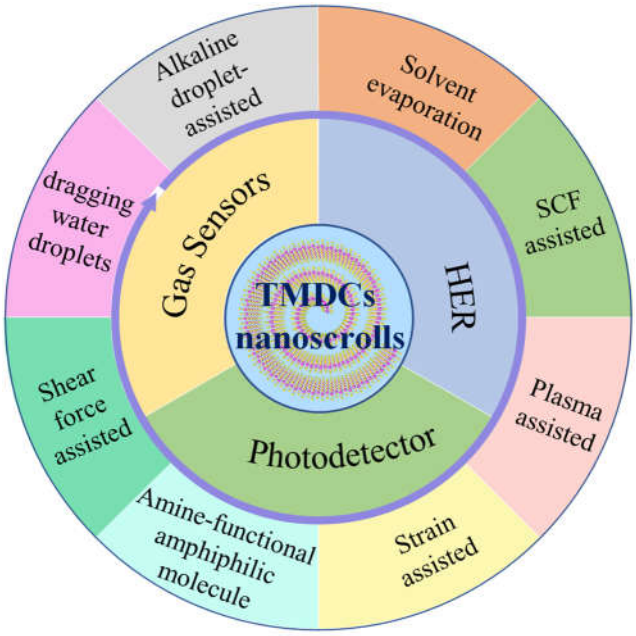

Figure 15. Summary of preparation and applications of TMDCs nanoscrolls.

Acknowledgments: This work was supported by the National Natural Science Foundation of China (Grant No. 51832001 and 21571101), the Natural Science Foundation of Jiangsu Province in China (Grant No. BK20161543), and the Natural Science Foundation of the Jiangsu Higher Education Institutions of China (Grant No. 15KJB430016).

References

1. Xuefei Zhou; Ziao Tian; Hyuk Jin Kim; Yang Wang; Borui Xu; Ruobing Pan; Young Jun Chang; Zengfeng Di; Peng Zhou; Mei, Y. Rolling up $MoSe_2$ nanomembranes as a sensitive tubular photodetector. *Small* **2019**, *15*, 1902528 -1902535, doi:10.1002/smll.201902528.
2. J, , M.; Wang G; Li X; Lu X; Zhang J; Yu H; Chen W; Du L; Liao M; J., Z.; et al. Rolling up a monolayer MoS_2 Sheet. *Small* **2016**, *12*, 3770-3774, doi:10.1002/smll.201601413.
3. Wang, L.; Yue, Q.; Pei, C.; Fan, H.; Dai, J.; Huang, X.; Li, H.; Huang, W. Scrolling bilayer WS_2/MoS_2 heterostructures for high-performance photo-detection. *Nano Res.* **2020**, *13*, 959-966, doi:10.1007/s12274-020-2725-9.
4. Chu, X.S.; Li, D.O.; Green, A.A.; Wang, Q.H. Formation of MoO_3 and WO_3 nanoscrolls from MoS_2 and WS_2 with atmospheric air plasma. *J. Mater. Chem. C* **2017**, *5*, 11301-11309, doi:10.1039/c7tc02867a.
5. Zhao, B.; Wan, Z.; Liu, Y.; Xu, J.; Yang, X.; Shen, D.; Zhang, Z.; Guo, C.; Qian, Q.; Li, J.; et al. High-order superlattices by rolling up van der Waals heterostructures. *Nature* **2021**, *591*, 385-390, doi:10.1038/s41586-021-03338-0.
6. Ghosh, R.; Lin, H.-I.; Chen, Y.-S.; Hofmann, M.; Hsieh, Y.-P.; Chen, Y.-F. Efficient light-confinement in heterostructured transition metal dichalcogenide-based nanoscrolls for high-performance photonic devices. *J. Mater. Res.* **2022**, *37*, 660-669, doi:10.1557/s43578-021-00460-7.
7. Fang, X.; Wei, P.; Wang, L.; Wang, X.; Chen, B.; He, Q.; Yue, Q.; Zhang, J.; Zhao, W.; Wang, J.; et al. Transforming monolayer transition-metal dichalcogenide nanosheets into one-dimensional nanoscrolls with high photosensitivity. *ACS Appl. Mater. Interfaces* **2018**, *10*, 13011-13018, doi:10.1021/acsami.8b01856.
8. Cui, X.; Kong, Z.; Gao, E.; Huang, D.; Hao, Y.; Shen, H.; Di, C.A.; Xu, Z.; Zheng, J.; Zhu, D. Rolling up transition metal dichalcogenide nanoscrolls via one drop of ethanol. *Nat. Commun.* **2018**, *9*, 1301-1308, doi:10.1038/s41467-018-03752-5.
9. Deng, W.; You, C.; Chen, X.; Wang, Y.; Li, Y.; Feng, B.; Shi, K.; Chen, Y.; Sun, L.; Zhang, Y. High-performance photodiode based on atomically thin WSe_2 /MoS_2 nanoscroll integration. *Small* **2019**, *15*, 1901544-1901550, doi:10.1002/smll.201901544.
10. Ji, E.; Son, J.; Kim, J.H.; Lee, G.-H. Rolling up two-dimensional sheets into nanoscrolls. *FlatChem* **2018**, *7*, 26-33, doi:10.1016/j.flatc.2017.09.002.
11. Su, J.; Li, X.; Xu, M.; Zhang, J.; Liu, X.; Zheng, X.; Shi, Y.; Zhang, Q. Enhancing photodetection ability of MoS_2 nanoscrolls via interface engineering. *ACS Appl. Mater. Interfaces* **2023**, *15*, 3307-3316, doi:10.1021/acsami.2c18537.
12. Du, L.; Hasan, T.; Castellanos-Gomez, A.; Liu, G.-B.; Yao, Y.; Lau, C.N.; Sun, Z. Engineering symmetry breaking in 2D layered materials. *Nat. Rev. Phys.* **2021**, *3*, 193-206, doi:10.1038/s42254-020-00276-0.
13. Lai, Z.; Chen, Y.; Tan, C.; Zhang, X.; Zhang, H. Self-assembly of two-dimensional nanosheets into one-dimensional nanostructures. *Chem.* **2016**, *1*, 59-77, doi:10.1016/j.chempr.2016.06.011.
14. Koppens, F.H.; Mueller, T.; Avouris, P.; Ferrari, A.C.; Vitiello, M.S.; Polini, M. Photodetectors based on graphene, other two-dimensional materials and hybrid systems. *Nat. Nanotechnol.* **2014**, *9*, 780-793, doi:10.1038/nnano.2014.215.
15. Long, M.; Wang, P.; Fang, H.; Hu, W. Progress, challenges, and opportunities for 2D material based photodetectors. *Adv. Funct. Mater.* **2018**, *29*, 1803807-1803835, doi:10.1002/adfm.201803807.
16. Huo, N.; Konstantatos, G. Recent progress and future prospects of 2D-based photodetectors. *Adv. Mater.* **2018**, *30*, 1801164-1081181, doi:10.1002/adma.201801164.
17. Deng, W.; Chen, X.; Li, Y.; You, C.; Chu, F.; Li, S.; An, B.; Ma, Y.; Liao, L.; Zhang, Y. Strain effect enhanced ultrasensitive MoS_2 nanoscroll avalanche photodetector. *J. Phys. Chem. Lett.* **2020**, *11*, 4490-4497, doi:10.1021/acs.jpclett.0c00861.
18. Chaoliang Tan; Xiehong Cao; Xue-Jun Wu; Qiyuan He; Jian Yang; Xiao Zhang; Junze Chen; Wei Zhao; Shikui Han; Gwang-Hyeon Nam; et al. Recent advances in ultrathin two-dimensional nanomaterials. *Chem. Rev.* **2017**, *117*, 6225–6331, doi:10.1021/acs.chemrev.6b00558.
19. Yue, Q.; Wang, L.; Fan, H.; Zhao, Y.; Wei, C.; Pei, C.; Song, Q.; Huang, X.; Li, H. Wrapping plasmonic silver nanoparticles inside one-dimensional nanoscrolls of transition-metal dichalcogenides for enhanced photoresponse. *Inorg. Chem.* **2021**, *60*, 4226-4235, doi:10.1021/acs.inorgchem.0c03235.
20. Da Young Hwang; Suh, D.H. Universal surface modification of transition metal dichalcogenide decorated with metal nanoparticles for surface enhanced Raman scattering. *Mater. Res. Bull.* **2017**, *90*, 73-80,

doi:10.1016/j.materresbull.2017.02.015.
21. Perim, E.; Machado, L.D.; Galvao, D.S. A brief review on syntheses, structures, and applications of nanoscrolls. *Front. Mater.* **2014**, *1*, 31-38, doi:10.3389/fmats.2014.00031.
22. Mariana C.F. Costa; Pei Rou Ng ; Sergey Grebenchuck ; Jun You Tan ; Gavin K.W. Koon ; Hui Li Tan; Colin R. Woods; Ricardo K. Donato; Kostya S. Novoselov; Neto, A.H.C. Colossal enhancement of electrical and mechanical properties of graphene nanoscrolls. *Carbon* **2023**, *208*, 140–147, doi:10.1016/j.carbon.2023.03.025.
23. Muschi, M.; Lalitha, A.; Sene, S.; Aureau, D.; Fregnaux, M.; Esteve, I.; Rivier, L.; Ramsahye, N.; Devautour-Vinot, S.; Sicard, C.; et al. Formation of a single-crystal aluminum-based MOF nanowire with graphene oxide nanoscrolls as structure-directing agents. *Angew. Chem. Int. Ed. Engl.* **2020**, *59*, 10353-10358, doi:10.1002/anie.202000795.
24. Wang, Y.; Jiang, C.; Chen, Q.; Zhou, Q.; Wang, H.; Wan, J.; Ma, L.; Wang, J. Highly promoted carrier mobility and intrinsic stability by rolling up monolayer black phosphorus into nanoscrolls. *J Phys. Chem. Lett.* **2018**, *9*, 6847-6852, doi:10.1021/acs.jpclett.8b02913.
25. Yitian Wang; Xuehao Tang; Qionghua Zhou; Xinyu Chen; Qian Chen ; Xu, Y. Blue phosphorus nanoscrolls. *Phys. Rev. B* **2020**, *102*, 165428-165434, doi:10.1103/PhysRevB.102.165428.
26. Miranti, R.; Qayyum, M.S.; Sharma, A.; Einarsrud, M.-A.; Mestres, N.; Benelmekki, M. Spectroscopic study of partially oxidized BN nanoscrolls induced by low frequency ultrasonic irradiation. *Appl. Surf. Sci.* **2020**, *515*, 146055-146062, doi:10.1016/j.apsusc.2020.146055.
27. Bacon, R. Growth, ctructure, and properties of graphite whiskers. *J. Appl. Phys.* **1960**, *31*, 283-290, doi:10.1063/1.1735559.
28. V. P. Dravid; X. Lin; Y. Wang; X. K. Wang; A. Yee; J. B. Ketterson; Chang, R.P.H. Buckytubes and derivatives their growth and implications for buckyball formation. *Science* **1993**, *259*, 1601-1604.
29. H Shioyama; Akita, T. A new route to carbon nanotubes. *Carbon* **2003**, *41*, 179–198.
30. Lisa M. Viculis; Julia J. Mack; Kaner, R.B. A chemical route to carbon nanoscrolls. *Science* **2003**, *299*, 1361.
31. Scheila F. Braga; Vitor R. Coluci; Sergio B. Legoas; Ronaldo Giro; Douglas S. Galvão; Baughman, R.H. Structure and dynamics of carbon nanoscrolls. *Nano Lett.* **2004**, *4*, 881–884.
32. Hwang, D.Y.; Choi, K.H.; Park, J.E.; Suh, D.H. Highly efficient hydrogen evolution reaction by strain and phase engineering in composites of Pt and MoS_2 nano-scrolls. *Phys. Chem. Chem. Phys.* **2017**, *19*, 18356-18365, doi:10.1039/c7cp03495d.
33. Hwang, D.Y.; Choi, K.H.; Park, J.E.; Suh, D.H. Highly thermal-stable paramagnetism by rolling up MoS_2 nanosheets. *Nanoscale* **2017**, *9*, 503-508, doi:10.1039/c6nr07975j.
34. Alharbi, T.M.D.; Elmas, S.; Alotabi, A.S.; Andersson, M.R.; Raston, C.L. Continuous flow fabrication of MoS_2 scrolls for electrocatalytic hydrogen evolution. *ACS Sustain. Chem. Eng.* **2022**, *10*, 9325-9333, doi:10.1021/acssuschemeng.2c01031.
35. Wu, Z.; Li, F.; Ye, H.; Huang, X.; Li, H. Decorating MoS_2 nanoscrolls with solution-processed PbI_2 nanocrystals for improved photosensitivity. *ACS Appl. Nano Mater.* **2022**, *5*, 15892-15901, doi:10.1021/acsanm.2c04113.
36. Zhao, Y.; You, H.; Li, X.; Pei, C.; Huang, X.; Li, H. Solvent-free preparation of closely packed MoS_2 nanoscrolls for improved photosensitivity. *ACS Appl. Mater. Interfaces* **2022**, *14*, 9515-9524, doi:10.1021/acsami.1c24291.
37. Wang, Z.; Wu, H.H.; Li, Q.; Besenbacher, F.; Zeng, X.C.; Dong, M. Self-scrolling MoS_2 metallic wires. *Nanoscale* **2018**, *10*, 18178-18185, doi:10.1039/c8nr04611e.
38. Liu, Z.; Gao, J.; Zhang, G.; Cheng, Y.; Zhang, Y.W. From two-dimensional nano-sheets to roll-up structures: expanding the family of nanoscroll. *Nanotechnology* **2017**, *28*, 385704, doi:10.1088/1361-6528/aa7bf8.
39. Wang, R.; Guo, S.; Li, Z.; Weller, D.; Quan, S.; Yu, J.; Wu, M.; Jiang, J.; Wang, Y.; Liu, R. Strong anisotropic optical properties by rolling up MoS_2 nanoflake. *J Phys. Chem. Lett.* **2022**, *13*, 8409-8415, doi:10.1021/acs.jpclett.2c02072.
40. Chithaiah, P.; Ghosh, S.; Idelevich, A.; Rovinsky, L.; Livneh, T.; Zak, A. Solving the "MoS_2 nanotubes" synthetic enigma and elucidating the route for their catalyst-free and scalable production. *ACS Nano* **2020**, *14*, 3004-3016, doi:10.1021/acsnano.9b07866.
41. Han, Y.; Zhou, J.; Dong, J. Electronic and magnetic properties of MoS_2 nanoribbons with sulfur line vacancy defects. *Appl. Surf. Sci.* **2015**, *346*, 470-476, doi:10.1016/j.apsusc.2015.02.016.
42. Jiao, Y.; Hafez, A.M.; Cao, D.; Mukhopadhyay, A.; Ma, Y.; Zhu, H. Metallic MoS_2 for high performance energy storage and energy conversion. *Small* **2018**, *14*, 1800640-1800660, doi:10.1002/smll.201800640.
43. Kotekar-Patil, D.; Deng, J.; Wong, S.L.; Lau, C.S.; Goh, K.E.J. Single layer MoS_2 nanoribbon field effect transistor. *Appl. Phys. Lett.* **2019**, *114*, 13508-13513, doi:10.1063/1.5079860.

44. Li, H.; Yin, Z.; He, Q.; Li, H.; Huang, X.; Lu, G.; Fam, D.W.; Tok, A.I.; Zhang, Q.; Zhang, H. Fabrication of single- and multilayer MoS_2 film-based field-effect transistors for sensing NO at room temperature. *Small* **2012**, *8*, 63-67, doi:10.1002/smll.201101016.
45. Ali Mehdizadeh ; Mahdieh Zeynali ; Karimi, M. Engineering of MoS_2 nanoribbons as high-performance materials for biosensing applications. *Appl. Surf. Sci.* **2021**, *540*, 148349-148359, doi:10.1016/j.apsusc.2020.148349.
46. Seravalli, L.; Bosi, M.; Fiorenza, P.; Panasci, S.E.; Orsi, D.; Rotunno, E.; Cristofolini, L.; Rossi, F.; Giannazzo, F.; Fabbri, F. Gold nanoparticle assisted synthesis of MoS_2 monolayers by chemical vapor deposition. *Nanoscale Advances* **2021**, *3*, 4826-4833, doi:10.1039/d1na00367d.
47. Wang, Q.; Sang, P.; Wei, W.; Li, Y.; Chen, J. Functionalized MoS_2 nanoribbons for intrinsic cold-source transistors: a computational study. *ACS Appl. Nano Mater.* **2022**, *5*, 1178-1184, doi:10.1021/acsanm.1c03793.
48. Wu, Z.; Li, F.; Li, X.; Yang, Y.; Huang, X.; Li, H. Direct synthesis of MoS_2 nanosheets in reduced graphene oxide nanoscroll for enhanced photodetection. *Nanomaterials (Basel)* **2022**, *12*, 1581-1591, doi:10.3390/nano12091581.
49. Yi, J.-D.; Liu, T.-T.; Huang, Y.-B.; Cao, R. Solid-state synthesis of MoS_2 nanorod from molybdenum-organic framework for efficient hydrogen evolution reaction. *Sci. China Mater.* **2019**, *62*, 965-972, doi:10.1007/s40843-018-9393-x.
50. Jeong, Y.; Shin, J.; Hong, Y.; Wu, M.; Hong, S.; Kwon, K.C.; Choi, S.; Lee, T.; Jang, H.W.; Lee, J.-H. Gas sensing characteristics of the FET-type gas sensor having inkjet-printed WS_2 sensing layer. *Solid State Electron.* **2019**, *153*, 27-32, doi:10.1016/j.sse.2018.12.009.
51. John M. Woods; Yeonwoong Jung; Yujun Xie; Wen Liu; Yanhui Liu; Hailiang Wang; Cha, J.J. One-step synthesis of MoS_2/WS_2 layered heterostructures and catalytic activity of defective transition metal dichalcogenide films. *ACS Nano* **2016**, *10*, 2004–2009, doi:10.1021/acsnano.5b06126.
52. Lin, C.; Cai, L.; Fu, J.H.; Sattar, S.; Wang, Q.X.; Wan, Y.; Tseng, C.C.; Yang, C.W.; Aljarb, A.; Jiang, K.; et al. Direct band gap in multilayer transition metal dichalcogenide nanoscrolls with enhanced photoluminescence. *Acs Mater Lett* **2022**, *4*, 1547-1555, doi:10.1021/acsmaterialslett.2c00162.
53. Pitchai Thangasamy; Jeyaraman Anandha Raj; Sathish, M. Transformation of multilayer WS_2 nanosheets to 1D luminescent WS_2 nanostructures by one-pot supercritical fluid processing for hydrogen evolution reaction. *Mater. Sci. Semicond. Process.* **2020**, *119*, 105167-105174, doi:10.1016/j.mssp.2020.105167.
54. Zhou, X.; Tian, Z.; Kim, H.J.; Wang, Y.; Xu, B.; Pan, R.; Chang, Y.J.; Di, Z.; Zhou, P.; Mei, Y. Rolling up $MoSe_2$ nanomembranes as a sensitive tubular photodetector. *Small* **2019**, *15*, 1902528-1902535, doi:10.1002/smll.201902528.
55. Sathish, M.; Mitani, S.; Tomai, T.; Honma, I. Supercritical fluid assisted synthesis of N-doped graphene nanosheets and their capacitance behavior in ionic liquid and aqueous electrolytes. *J. Mater. Chem. A* **2014**, *2*, 4731-4738, doi:10.1039/c3ta15136k.
56. Zhang, S.; Gao, F.; Feng, W.; Yang, H.; Hu, Y.; Zhang, J.; Xiao, H.; Li, Z.; Hu, P. High-responsivity photodetector based on scrolling monolayer MoS_2 hybridized with carbon quantum dots. *Nanotechnology* **2021**, *33*, 105301-105309, doi:10.1088/1361-6528/ac3ce1.
57. Xu, J.; Jiang, H.; Shen, Y.; Li, X.Z.; Wang, E.G.; Meng, S. Transparent proton transport through a two-dimensional nanomesh material. *Nat. Commun.* **2019**, *10*, 3971-3979, doi:10.1038/s41467-019-11899-y.
58. Graba, M.; Mamala, J.; Bieniek, A.; Sroka, Z. Impact of the acceleration intensity of a passenger car in a road test on energy consumption. *Energy* **2021**, *226*, 120429-120445, doi:10.1016/j.energy.2021.120429.
59. Yang, J.; Zeng, Z.; Kang, J.; Betzler, S.; Czarnik, C.; Zhang, X.; Ophus, C.; Yu, C.; Bustillo, K.; Pan, M.; et al. Formation of two-dimensional transition metal oxide nanosheets with nanoparticles as intermediates. *Nat. Mater.* **2019**, *18*, 970-976, doi:10.1038/s41563-019-0415-3.
60. Gentile, P.; Cuoco, M.; Volkov, O.M.; Ying, Z.-J.; Vera-Marun, I.J.; Makarov, D.; Ortix, C. Electronic materials with nanoscale curved geometries. *Nat. Electron.* **2022**, *5*, 551-563, doi:10.1038/s41928-022-00820-z.
61. Xu, C.; Wu, X.; Huang, G.; Mei, Y. Rolled-up nanotechnology: materials issue and geometry capability. *Adv. Mater. Technol.* **2018**, *4*, 1800486-1800512, doi:10.1002/admt.201800486.
62. Cho, J.H.; Azam, A.; Gracias, D.H. Three dimensional nanofabrication using surface forces. *Langmuir* **2010**, *26*, 16534-16539, doi:10.1021/la1013889.
63. Li, J.; Zhang, J.; Gao, W.; Huang, G.; Di, Z.; Liu, R.; Wang, J.; Mei, Y. Dry-released nanotubes and nanoengines by particle-assisted rolling. *Adv. Mater.* **2013**, *25*, 3715-3721, doi:10.1002/adma.201301208.
64. Huang, X.; Huang, Z.; Liu, Q.; Zhou, A.a.; Ma, Y.; Wang, J.; Qiu, H.; Bai, H. Organic solvent-assisted lyophilization: a universal method of preparing two-dimensional material nanoscrolls. *ACS Omega* **2019**, *4*, 7420-7427, doi:10.1021/acsomega.9b00623.
65. Ghosh, R.; Lin, H.I.; Chen, Y.S.; Singh, M.; Yen, Z.L.; Chiu, S.; Lin, H.Y.; Bera, K.P.; Liao, Y.M.; Hofmann,

M.; et al. QD/2D hybrid nanoscrolls: a new class of materials for high-performance polarized photodetection and ultralow threshold laser action. *Small* **2020**, *16*, 2003944-2003953, doi:10.1002/smll.202003944.
66. Jeonghyeon Na; Changyeon Park ; Chang Hoi Lee; Won Ryeol Choi; Sooho Choi; Jae-Ung Lee; Woochul Yang ; Hyeonsik Cheong; B., E.E.; Jhang, C.a.S.H. Indirect band gap in scrolled MoS_2 monolayers. *Nanomaterials* **2022**, *12*, 3353, doi:10.3390/nano12193353.
67. Hwang, D.Y.; Choi, K.H.; Suh, D.H. A vacancy-driven phase transition in MoX_2 (X: S, Se and Te) nanoscrolls. *Nanoscale* **2018**, *10*, 7918-7926, doi:10.1039/c7nr08634b.
68. Hwang, D.Y.; Suh, D.H. Evolution of a high local strain in rolling up MoS_2 sheets decorated with Ag and Au nanoparticles for surface-enhanced Raman scattering. *Nanotechnology* **2017**, *28*, 25603-25614, doi:10.1088/1361-6528/28/2/025603.
69. Janardhana Reddy ; G Basha, H.; Venkata Narayanan, N.S. Heat flow visualization of a chemical compound isobutane (C_4H_{10}) past a vertical cylinder in the subcritical, near critical and supercritical regions. *J. Mol. Struct.* **2018**, *259*, 209-219, doi:10.1016/j.molliq.2018.02.103.
70. L. El Khouri; Carle`s, P. Supercritical fluids as experimental models for geophysical flows. *Int J Thermophys* **2003**, *24*, 683-693.
71. Parag S. Shah; Tobias Hanrath; Keith P. Johnston; Korgel, B.A. Nanocrystal and nanowire synthesis and dispersibility in supercritical fluids. *J. Phys. Chem. B* **2004**, *108*, 9574-9587.
72. Schienbein, P.; Marx, D. Assessing the properties of supercritical water in terms of structural dynamics and electronic polarization effects. *Phys. Chem. Chem. Phys.* **2020**, *22*, 10462-10479, doi:10.1039/c9cp05610f.
73. Pitchai Thangasamy; Sathish, M. Rapid, one-pot synthesis of luminescent MoS_2 nanoscrolls using supercritical fluid processing. *J. Mater. Chem. C* **2016**, *4*, 1165-1169, doi:10.1039/c5tc03630e.
74. Thangasamy, P.; Sathish, M. Supercritical fluid processing: a rapid, one-pot exfoliation process for the production of surfactant-free hexagonal boron nitride nanosheets. *CrystEngComm* **2015**, *17*, 5895-5899, doi:10.1039/c5ce00926j.
75. Wang, W.; Gai, Y.; Xiao, D.; Zhao, Y. A facile and general approach for production of nanoscrolls with high-yield from two-dimensional nanosheets. *Sci. Rep.* **2018**, *8*, 15262-15268, doi:10.1038/s41598-018-33709-z.
76. Rangappa, D.; Sone, K.; Wang, M.; Gautam, U.K.; Golberg, D.; Itoh, H.; Ichihara, M.; Honma, I. Rapid and direct conversion of graphite crystals into high-yielding, good-quality graphene by supercritical fluid exfoliation. *Chem. Eur. J.* **2010**, *16*, 6488-6494, doi:10.1002/chem.201000199.
77. Alharbi, T.M.D.; Jellicoe, M.; Luo, X.; Vimalanathan, K.; Alsulami, I.K.; Al Harbi, B.S.; Igder, A.; Alrashaidi, F.A.J.; Chen, X.; Stubbs, K.A.; et al. Sub-micron moulding topological mass transport regimes in angled vortex fluidic flow. *Nanoscale Adv.* **2021**, *3*, 3064-3075, doi:10.1039/d1na00195g.
78. Vimalanathan, K.; Suarez-Martinez, I.; Peiris, M.C.R.; Antonio, J.; de Tomas, C.; Zou, Y.; Zou, J.; Duan, X.; Lamb, R.N.; Harvey, D.P.; et al. Vortex fluidic mediated transformation of graphite into highly conducting graphene scrolls. *Nanoscale Adv.* **2019**, *1*, 2495-2501, doi:10.1039/c9na00184k.
79. Al-Antaki, A.H.M.; Luo, X.; Alharbi, T.M.D.; Harvey, D.P.; Pye, S.; Zou, J.; Lawrance, W.; Raston, C.L. Inverted vortex fluidic exfoliation and scrolling of hexagonal-boron nitride. *RSC. Adv.* **2019**, *9*, 22074-22079, doi:10.1039/c9ra03970h.
80. Gaoshan Huang ; Mei, Y. Thinning and shaping solid films into functional and integrative nanomembranes. *Adv. Mater.* **2012**, *24*, 2517-2546, doi:10.1002/adma.201200574.
81. Song Hao; Bingchu Yang; Gao, Y. Fracture-induced nanoscrolls from CVD-grown monolayer molybdenum disulfide. *Phys. Status Solidi Rapid Res. Lett.* **2016**, *10*, 549-553, doi:10.1002/pssr.201600114.
82. Qian, Q.; Zu, R.; Ji, Q.; Jung, G.S.; Zhang, K.; Zhang, Y.; Buehler, M.J.; Kong, J.; Gopalan, V.; Huang, S. Chirality-dependent second harmonic generation of MoS_2 nanoscroll with enhanced efficiency. *ACS Nano* **2020**, *14*, 13333-13342, doi:10.1021/acsnano.0c05189.
83. Fan, X.; Su, L.; Zhang, F.; Huang, D.; Sang, D.K.; Chen, Y.; Li, Y.; Liu, F.; Li, J.; Zhang, H.; et al. Layer-dependent properties of ultrathin ges nanosheets and application in uv–vis photodetectors. *ACS Appl. Mater. Interfaces* **2019**, *11*, 47197-47206, doi:10.1021/acsami.9b14663.
84. Carlos G. Morales-Guio; Lucas-Alexandre Sterna; Hu, X. Nanostructured hydrotreating catalysts for electrochemical hydrogen evolution. *Chem. Soc. Rev.* **2014**, *43*, 6555-6569, doi:10.1039/c3cs60468c.
85. Zhou, X.; Lin, S.H.; Yang, X.; Li, H.; Hedhili, M.N.; Li, L.J.; Zhang, W.; Shi, Y. MoSx-coated NbS_2 nanoflakes grown on glass carbon: an advanced electrocatalyst for the hydrogen evolution reaction. *Nanoscale* **2018**, *10*, 3444-3450, doi:10.1039/c7nr09172a.
86. Li, H.; Jia, X.; Zhang, Q.; Wang, X. Metallic transition-metal dichalcogenide nanocatalysts for energy conversion. *Chem* **2018**, *4*, 1510-1537, doi:10.1016/j.chempr.2018.03.012.
87. Miika Mattinen; Markku Leskelä; Ritala, M. Atomic layer deposition of 2D metal dichalcogenides for

electronics, catalysis, energy storage, and beyond. *Adv. Mater. Interfaces* **2021**, *8*, 2001677-2001724, doi:10.1002/admi.202001677.

88. Wei Wang; Yutong Li; Mengjia Li; Hailin Shen; Wei Zhang; Jintao Zhang; Tianyu Liu; Kong, X.; Bi, H. Metallic phase WSe_2 nanoscrolls for the hydrogen evolution reaction. *New J. Chem.* **2022**, *46*, 8381–8384, doi:10.1039/D2NJ01598F.
89. Berit Hinnemann; Poul Georg Moses; Jacob Bonde; Kristina P. Jørgensen; Jane H. Nielsen; Sebastian Horch; Ib Chorkendorff; Nørskov, J.K. Biomimetic hydrogen evolution: MoS_2 nanoparticles as catalyst for hydrogen evolution. *J. Am. Chem. Soc.* **2005**, *127*, 5308-5309.
90. Wang, F.; Shifa, T.A.; Zhan, X.; Huang, Y.; Liu, K.; Cheng, Z.; Jiang, C.; He, J. Recent advances in transition-metal dichalcogenide based nanomaterials for water splitting. *Nanoscale* **2015**, *7*, 19764–19788, doi:10.1039/c5nr06718a.
91. Thomas F. Jaramillo; Kristina P. Jørgensen; Jacob Bonde; Jane H. Nielsen; Sebastian Horch; Chorkendorff, I. Identification of active edge sites for electrochemical H_2 evolution from MoS_2 nanocatalysts. *science* **2007**, *317*, 100-102.
92. Yan, Y.; Xia, B.; Xu, Z.; Wang, X. Recent development of molybdenum sulfides as advanced electrocatalysts for hydrogen evolution reaction. *ACS Catal.* **2014**, *4*, 1693-1705, doi:10.1021/cs500070x.
93. Henckel, D.A.; Lenz, O.M.; Krishnan, K.M.; Cossairt, B.M. Improved HER catalysis through facile, aqueous electrochemical activation of nanoscale WSe_2. *Nano Lett.* **2018**, *18*, 2329-2335, doi:10.1021/acs.nanolett.7b05213.
94. Damien Voiry; Jieun Yang; Chhowalla, M. Recent strategies for improving the catalytic activity of 2D TMD nanosheets toward the hydrogen evolution reaction. *Adv. Mater.* **2016**, *28*, 6197–6206, doi:10.1002/adma.201505597.
95. Lu, Q.; Yu, Y.; Ma, Q.; Chen, B.; Zhang, H. 2D transition-metal-dichalcogenide-nanosheet-based composites for photocatalytic and electrocatalytic hydrogen evolution reactions. *Adv. Mater.* **2016**, *28*, 1917-1933, doi:10.1002/adma.201503270.
96. Yuan, J.; Wu, J.; Hardy, W.J.; Loya, P.; Lou, M.; Yang, Y.; Najmaei, S.; Jiang, M.; Qin, F.; Keyshar, K.; et al. Facile synthesis of single crystal vanadium disulfide nanosheets by chemical vapor deposition for efficient hydrogen evolution reaction. *Adv. Mater.* **2015**, *27*, 5605-5609, doi:10.1002/adma.201502075.
97. Jiang, Z.; Zhou, W.; Hu, C.; Luo, X.; Zeng, W.; Gong, X.; Yang, Y.; Yu, T.; Lei, W.; Yuan, C. Interlayer-confined NiFe dual atoms withinMoS_2 electrocatalyst for ultra-efficient acidic overall water splitting. *Adv. Mater.* **2023**, 10.1002/adma.202300505, 2300505, doi:10.1002/adma.202300505.
98. Rheehyun Kim; Ji-Soo Jang; Dong-Ha Kim; Joon-Young Kang; Hee-Jin Cho; Yong Jin Jeong; Kim, I.-D. A general synthesis of crumpled metal oxide nanosheets as superior chemiresistive. *Adv. Funct. Mater.* **2019**, *29*, 1903128, doi:10.1002/adfm.201903128.
99. Atanu Bag ; Lee, N.-E. Gas sensing with heterostructures based on two-dimensional nanostructured materials a review. *J. Mater. Chem. C* **2019**, *7*, 13367-13383, doi:10.1039/c9tc04132j.
100. Kumar, R.; Goel, N.; Hojamberdiev, M.; Kumar, M. Transition metal dichalcogenides-based flexible gas sensors. *Sens. Actuator A Phys.* **2020**, *303*, 111875-111902, doi:10.1016/j.sna.2020.111875.
101. Goswami, P.; Gupta, G. Recent progress of flexible NO_2 and NH_3 gas sensors based on transition metal dichalcogenides for room temperature sensing. *Mater. Today Chem.* **2022**, *23*, 100726-100739, doi:10.1016/j.mtchem.2021.100726.
102. Liu, J.; Hu, Z.; Zhang, Y.; Li, H.Y.; Gao, N.; Tian, Z.; Zhou, L.; Zhang, B.; Tang, J.; Zhang, J.; et al. MoS_2 nanosheets sensitized with quantum dots for room-temperature gas sensors. *Nanomicro Lett* **2020**, *12*, 59-72, doi:10.1007/s40820-020-0394-6.
103. P. Bharathi; S. Harish, M.; Shimomura; S. Ponnusamy; M. Krishna Mohan; J. Archana; Navaneethan, M. Conductometric NO_2 gas sensor based on Co-incorporated MoS_2 nanosheets for room temperature applications. *Sens. Actuators B Chem.* **2022**, *360*, 131600, doi:10.1016/j.snb.2022.131600.
104. Bai, H.; Guo, H.; Feng, C.; Wang, J.; Liu, B.; Xie, Z.; Guo, F.; Chen, D.; Zhang, R.; Zheng, Y. Light-activated ultrasensitive NO_2 gas sensor based on heterojunctions of CuO nanospheres/MoS_2 nanosheets at room temperature. *Sens. Actuators B Chem.* **2022**, *368*, 132131-132146, doi:10.1016/j.snb.2022.132131.

105. Zhang, L.; Hao, Q.; Liu, J.; Zhou, J.; Zhang, W.; Li, Y. Rolling up of 2D nanosheets into 1D Nanoscrolls: visible-light-activated chemiresistors based on surface modified indium selenide with enhanced sensitivity and stability. *Chem. Eng. J.* **2022**, *446*, 136937-136911, doi:10.1016/j.cej.2022.136937.
106. Park, H.; Park, J.; Kang, S.-W.; Jeong, S.-H. 3D-nanostructured MoS_2 nanoscroll with highly active sites for improving NO_2 gas detection. *Mater. Lett.* **2023**, *349*, 134733-134737, doi:10.1016/j.matlet.2023.134733.